Multiparametric Electromagnetic Inversion of 3-D Anisotropic Objects Embedded in Layered Media Based on Mixed L_1–L_2 Norm Regularization

Yanjin Chen, Jiawen Li, Lixiao Wang, Feng Han, *Senior Member, IEEE*, and Qing Huo Liu, *Fellow, IEEE*

***Abstract*—In this letter, the mixed L_1–L_2 norm regularization is adopted to constrain the full-wave inversion solution of the multiparametric electromagnetic inverse scattering by the 3-D anisotropic objects. The mixed L_1–L_2 regularization term is added to the standard L_2 norm cost function in the framework of the Born iterative method. In each iteration, the mixed L_1–L_2 norm term is transformed into L_2 norm term through a weight matrix and the whole cost function is minimized by the conjugate gradient method. Numerical results show that, compared with the traditional Tikhonov L_2 regularization, the mixed L_1–L_2 regularization can achieve higher reconstruction accuracy without additional computational cost due to the structural similarity constraint among different model parameters.**

***Index Terms*—Electromagnetic (EM) inverse scattering, full-wave inversion (FWI), mixed L_1–L_2 norm regularization.**

I. Introduction

ELECTROMAGNETIC (EM) inverse scattering theory has been developed rapidly in recent decades and has been widely applied in various fields, such as breast cancer diagnostics [1], nondestructive evaluation [2], through-wall imaging [3], and so on. In many full-wave inversion (FWI) application scenarios like composite laminates scattering [4], hydraulic fracture mapping [5], EM well-logging [6], and microwave device design [7], the anisotropy of the dielectric parameters must be taken into account.

Due to the ill-posedness of the EM inverse scattering problems, especially for the anisotropic scatterers with multiple model parameters to be reconstructed, regularization is necessary for the FWI to obtain meaningful solutions. Researchers have proposed several regularization techniques to alleviate the ill-posedness by restricting the solution ranges and incorporating prior information. The widely used regularization is the Tikhonov L_2 norm term of the model parameter vector, which is usually directly added to the L_2 norm cost function [8]. Such a direct constraint can effectively prevent the solutions from having infinite large values and avoid their nonuniqueness. In addition, because the L_2 norm term is differentiable everywhere, it is straightforward to implement the minimization of the regularized cost function. However, the solution based on L_2 norm regularization is smooth and the boundaries of the reconstructed scatterers are blurred [9]. By contrast, the L_1 norm regularization has the natural advantage to capture the sharp boundaries of the scatterers [10]. It is based on the prior information of the sparse solution and widely employed in compressive sensing. Unfortunately, due to the assumption that the solution is sparse, the EM FWI based on L_1 norm regularization is suitable for point-like scatterers or small-size scatterers [11]. Another limitation of L_1 norm regularization, when applied to compressive sensing, is that the Fréchet derivative matrix must meet the requirement of the restricted isometric property[12]. The total variation (TV) regularization can maintain both the interior smoothness of a scatterer and its sharp boundary, by minimizing the L_1 norm of the spatial gradients of the model parameters. It is widely adopted in many EM FWI methods, e.g., contrast source inversion[13]. Shah *et al.* [14] proposed a joint L_1–L_2 norm regularization by adding the L_1 and L_2 norm terms together. It was shown that this joint method can obtain the solutions without oversmoothening at discontinuities but preserve the sufficient condition for the sparse recovery [14]. The minimum support (MS) regularization proposed by Portniaguine and Zhdanov [15], [16] proved to be capable of focusing inversion images and generating sharp boundaries.

The aforementioned regularization schemes have been successfully applied in the reconstruction of the isotropic scatterers. To our knowledge, the L_2 norm regularization is commonly used in the EM inversion of anisotropic scatterers since it is easy to implement and needs no additional computational cost. For example, Sun [17] used the cost function based on the L_2 norm regularization to retrieve the anisotropic permittivities. Since all the dielectric parameters of the anisotropic scatterer share the same geometric structure, we use the mixed L_1–L_2 norm regularization to constrain the solution of the EM inversion in this letter. The L_2 norm constraint is imposed on all the different dielectric parameters in a certain discretized cell, while the L_1 norm constraint is imposed on all the L_2 norm values in all the discretized cells. As a result, the mixed L_1–L_2 norm can force all the different dielectric parameters in a cell to approach zero simultaneously, which realizes the shape consistency constraint among different parameters. In contrast, the joint L_1–L_2 norm regularization proposed in [14] is to find the focused shape for the reconstruction by directly adding the L_1 and the L_2 norm terms

Manuscript received January 19, 2021; revised February 18, 2021; accepted February 21, 2021. Date of publication February 23, 2021; date of current version May 5, 2021. This work was supported by the National Key Research and Development Program of the Ministry of Science and Technology of China under Grant 2018YFF01013300. *(Corresponding author: Feng Han.)*

Yanjin Chen, Jiawen Li, Lixiao Wang, and Feng Han are with the Key Laboratory of Electromagnetic Wave Science and Detection Technology, Institute of Electromagnetics and Acoustics, Xiamen University, Xiamen 361005, China (e-mail: feng.han@xmu.edu.cn).

Qing Huo Liu is with the Department of Electrical and Computer Engineering, Duke University, Durham, NC 27708 USA (e-mail: qhliu@duke.edu).

Digital Object Identifier 10.1109/LAWP.2021.3061652

together. The purpose of the L_1 norm is to focus the shape, while that of the L_2 norm is to offset the L_1 norm effect in case the solution is too sparse. Similarly, the MS regularization in [15] and [16] is also to find focused images and sharp boundaries instead of forcing different parameters sharing the same shape.

The rest of the letter is organized as follows. In Section II, the forward and inversion models for the FWI and the mixed L_1–L_2 norm regularization are described in detail. In Section III, a numerical example is used to verify the proposed method. Finally, Section IV concludes this letter.

II. Methods

A. Forward and Inversion Models

The EM scattering model for scatterers embedded in layered media is commonly used for subsurface detection [18], or through-wall imaging [3]. The forward model is formulated by the following state equation:

$$\mathbf{E}_{\text{inc}}(\mathbf{r}) = \mathbf{E}_{\text{tot}}(\mathbf{r}) - j\omega\varepsilon_0 \int_D \overline{\overline{\mathbf{G}}}_{\mathbf{EJ}}(\mathbf{r},\mathbf{r}')[\bar{\bar{\epsilon}}_s(\mathbf{r}') - \bar{\bar{\epsilon}}_b(\mathbf{r}')]\mathbf{E}_{\text{tot}}(\mathbf{r}')d\mathbf{r}' \quad (1)$$

where $\mathbf{E}_{\text{inc}}$ is the incident field in the inversion domain when the 3-D arbitrary anisotropic scatterer is absent, while $\mathbf{E}_{\text{tot}}$ is the total field when the scatterer is present. $\overline{\overline{\mathbf{G}}}_{\mathbf{EJ}}$ is the dyadic Green's function in layered uniaxial anisotropic media [19], linking the source point $\mathbf{r}'$ and the field point $\mathbf{r}$. The inversion model is formulated by the following data equation:

$$\mathbf{E}_{\text{sct}}(\mathbf{r}) = j\omega\varepsilon_0 \int_D \overline{\overline{\mathbf{G}}}_{\mathbf{EJ}}(\mathbf{r},\mathbf{r}')[\bar{\bar{\epsilon}}_s(\mathbf{r}') - \bar{\bar{\epsilon}}_b(\mathbf{r}')]\mathbf{E}_{\text{tot}}(\mathbf{r}')d\mathbf{r}' \quad (2)$$

where $\mathbf{E}_{\text{sct}}$ is the scattered electric field measured at the receiver array, $\bar{\bar{\epsilon}}_b$ is the diagonal tensor of the complex permittivity of the background medium with the uniaxial anisotropy, and $\bar{\bar{\epsilon}}_s$ is the symmetrical full tensor of the complex permittivity of the scatterer with the arbitrary anisotropy. In this letter, we only consider the symmetrical tensor of the scatterer, which is ubiquitous in nature [6]. The expression $\bar{\bar{\epsilon}}_s$ can be found in [20]. Therefore, there are 12 unknowns (six for permittivity and six for conductivity) to reconstruct in the inversion. In the forward computation, (1) is discretized based on the roof-top basis functions [21] and the stabilized biconjugate-gradient fast Fourier transform (BCGS-FFT) [22] is adopted to solve $\mathbf{E}_{\text{tot}}$. In the inversion, (2) is discretized and the Born iterative method (BIM) [23] is used to solve $\bar{\bar{\epsilon}}_s$.

B. Mixed L_1–L_2 Norm Regularization

The cost function of the BIM with the regularization term is constructed as

$$f(\mathbf{x}) = \frac{1}{2}\|\mathbf{A}\mathbf{x} - \mathbf{b}\|_2^2 + \gamma R(\mathbf{x}) \quad (3)$$

where

$$\mathbf{x} = \left[\underbrace{x_{11}, x_{12}\cdots x_{1\,M}}_{\mathbf{x}_1^{\mathrm{T}}}\cdots\underbrace{x_{i1}\cdots x_{iM}}_{\mathbf{x}_i^{\mathrm{T}}}\cdots\underbrace{x_{N1}\cdots x_{NM}}_{\mathbf{x}_N^{\mathrm{T}}}\right]^{\mathrm{T}} \quad (4)$$

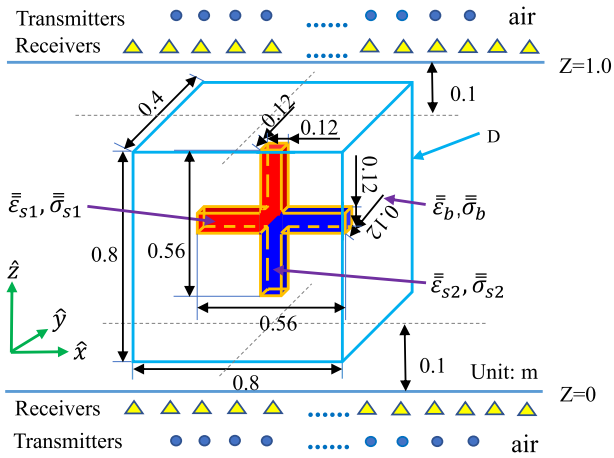

Fig. 1. Configuration of the inversion model with an inhomogeneous cross shape embedded in the middle layer.

is the unknown vector including all the dielectric parameters in all the discretized cells, $\mathbf{x}_i$ is a column vector including all the different dielectric parameters in a certain discretized cell, N is the number of discretized cells in the whole inversion domain, $M = 12$ is the number of the unknown model parameters in a cell, $\mathbf{A}$ is the Fréchet derivative matrix, $\mathbf{b}$ is the measured data vector, γ is the regularization factor, $\|\cdot\|_2^2$ denotes the L_2 norm, and T denotes the matrix transpose. If we choose the Tikhonov L_2 norm regularization, i.e., let $R(\mathbf{x}) = \|\mathbf{x}\|_2^2$, all model parameters in $\mathbf{x}$ are independent of each other in the solution. Therefore, the reconstructed geometric shapes of the scatterer for different anisotropic parameters are not necessarily the same. However, if we choose the mixed L_1–L_2 norm regularization, i.e., let

$$R(\mathbf{x}) = \|\mathbf{x}\|_{1,2} = \sum_{i=1}^{N}\sqrt{\sum\nolimits_{j=1}^{M} x_{i,j}^2} \quad (5)$$

the L_2 norm of all the different dielectric parameters in a certain discretized cell is constrained by the L_1 norm. In other words, all the dielectric parameters in a cell take the zero values simultaneously. As a result, the reconstructed shapes of the scatterer for different anisotropic parameters are the same. Because the L_1 norm in (5) is not differentiable everywhere, we transform the L_1–L_2 norm into the L_2 norm by using the weight matrix

$$\|\mathbf{x}\|_{1,2} = \frac{1}{2}\sum_{i=1}^{N}\left\|\mathbf{W}_i^{\frac{1}{2}}\mathbf{x}_i\right\|_2^2 = \frac{1}{2}\left\|\widetilde{\mathbf{W}}^{\frac{1}{2}}\mathbf{x}\right\|_2^2 = \frac{1}{2}\left\|\begin{pmatrix}\mathbf{W}_1^{\frac{1}{2}} & \cdots & 0\\ \vdots & \ddots & \vdots\\ 0 & \cdots & \mathbf{W}_N^{\frac{1}{2}}\end{pmatrix}\begin{pmatrix}\mathbf{x_1}\\ \vdots\\ \mathbf{x}_N\end{pmatrix}\right\|_2^2 \quad (6)$$

where $\mathbf{W}_i = \mathrm{diag}\{2(\sum_{j=1}^{M} x_{i,j}^2 + \delta)^{-\frac{1}{2}}\}$ is the weight matrix and δ is a small number, which is used to prevent the denominator from being equal to zero. A similar technique has been successfully adopted to transform the TV regularization into the L_2 norm, and its key point is to transform any L_p norm into the L_2 norm by selecting the proper power of the unknown model parameters and placing them in the diagonal elements of the weight matrix [24]. Once $\|\mathbf{x}\|_{1,2}$ is transformed

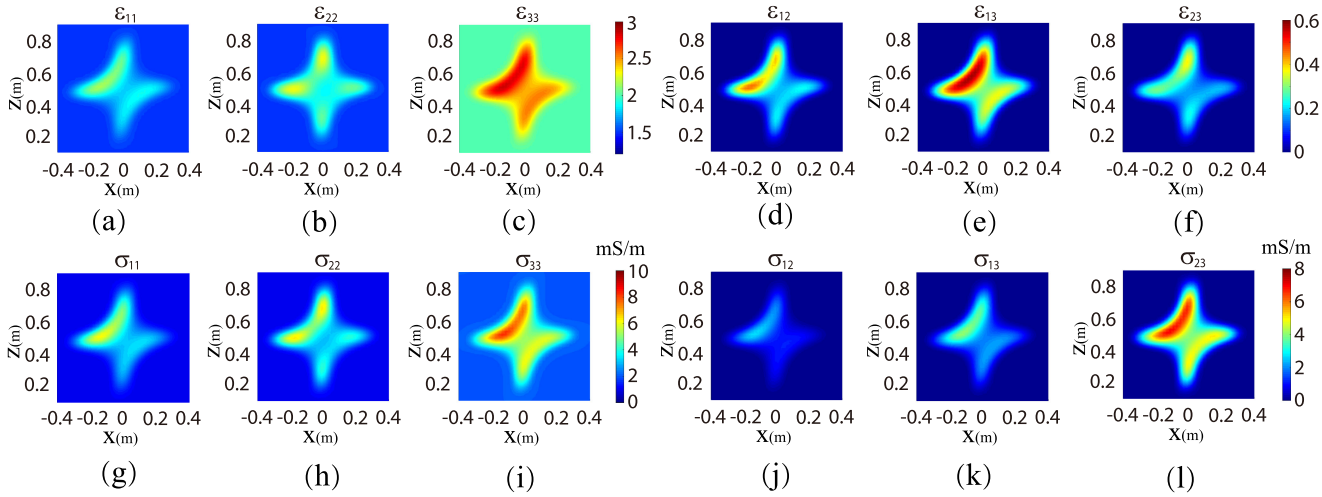

Fig. 2. 2-D slices at $y = 0$ of the reconstructed dielectric parameters obtained by the BIM with the mixed L_1–L_2 norm regularization.

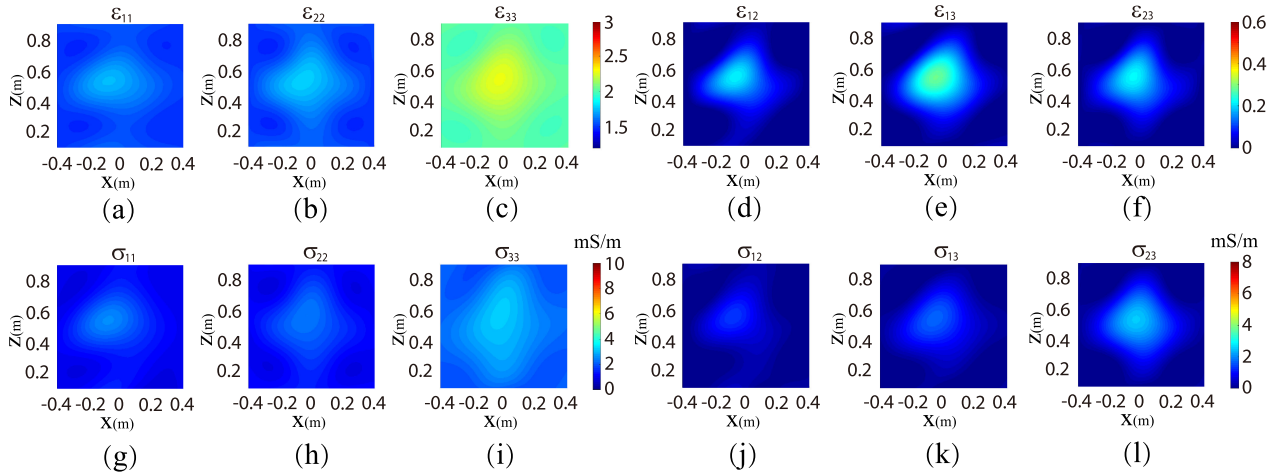

Fig. 3. 2-D slices at $y = 0$ of the reconstructed dielectric parameters obtained by the BIM with the L_2 norm regularization.

into the L_2 norm form, the cost function in (3) can be easily minimized by the conjugate gradient (CG) method. Compared with the inversion based on the L_2 norm regularization, the additional computational cost of the mixed L_1–L_2 regularization is the evaluation of the weight matrix $\widetilde{\mathbf{W}}$. However, because it only needs some simple arithmetic operations, the cost can be ignored.

III. Numerical Results

In this section, the numerical simulation is implemented to verify the mixed L_1–L_2 norm regularization. The scatterer is an inhomogeneous cross shape and is arbitrarily anisotropic with the symmetrical dielectric tensors. It is placed in the middle layer, and the transmitter and receiver arrays are placed in the top and bottom layers, respectively, as shown in Fig. 1. The sizes of the inversion domain D and the scatterer are also labeled in Fig. 1. The dielectric parameter values are listed in Table I. The operating frequency is 300 MHz. The 128 transmitters are uniformly located in two 2.8×1.4 m planes at $z = -0.2$ m and $z = 1.2$ m, respectively. The interval between the two transmitters is 0.4 m in the $\hat{x}$-direction but 0.2 m in the $\hat{y}$-direction. The scattered fields are collected by 162 receivers' arrays uniformly located in two 4.0×2.0 m planes at $z = -0.1$ m and $z = 1.1$ m, respectively. The interval between two receivers is 0.5 m in the $\hat{x}$-direction but 0.25 m in the $\hat{y}$-direction. The layouts of the transmitter and receiver arrays roughly follow the Nyquist law, i.e., each transmitter or receiver is placed in a half-wavelength interval. The interval in the $\hat{x}$-direction is larger than that in the $\hat{y}$-direction because the scatterer is larger in the $\hat{x}$-direction. This configuration guarantees good inversion results but avoids oversampling. In addition, the transmitter is an infinitesimal dipole and the effect of its radiation pattern on

TABLE I
Relative Permittivity and Conductivity of the Background Medium and the Cross Shape

	ε_{11}	ε_{12}	ε_{13}	ε_{22}	ε_{23}	ε_{33}	σ_{11}	σ_{12}	σ_{13}	σ_{22}	σ_{23}	σ_{33}
$\overline{\overline{\varepsilon}}_b$ $\overline{\overline{\sigma}}_b$	1.5	0.0	0.0	1.5	0.0	2.0	1.0	0.0	0.0	1.0	0.0	2.0
$\overline{\overline{\varepsilon}}_{s1}$ $\overline{\overline{\sigma}}_{s1}$	2.0	0.4	0.5	2.3	0.4	2.8	5.0	3.0	4.0	6.0	7.0	8.0
$\overline{\overline{\varepsilon}}_{s2}$ $\overline{\overline{\sigma}}_{s2}$	1.8	0.2	0.3	2.0	0.2	2.5	3.0	1.0	2.0	4.0	5.0	6.0

Remark: the unit of σ is mS/m.

TABLE II
SSIMs BETWEEN THE RECONSTRUCTED PARAMETERS AND GROUND TRUTHS BASED ON TWO TYPES OF REGULARIZATION

	ε_{11}	ε_{12}	ε_{13}	ε_{22}	ε_{23}	ε_{33}	σ_{11}	σ_{12}	σ_{13}	σ_{22}	σ_{23}	σ_{33}
mixed L_1-L_2	0.8563	0.8554	0.8517	0.8325	0.8309	0.8270	0.8511	0.8395	0.8365	0.8381	0.8229	0.8189
L_2	0.5949	0.5464	0.5987	0.5334	0.5161	0.5792	0.6271	0.5294	0.5451	0.5809	0.5574	0.5887

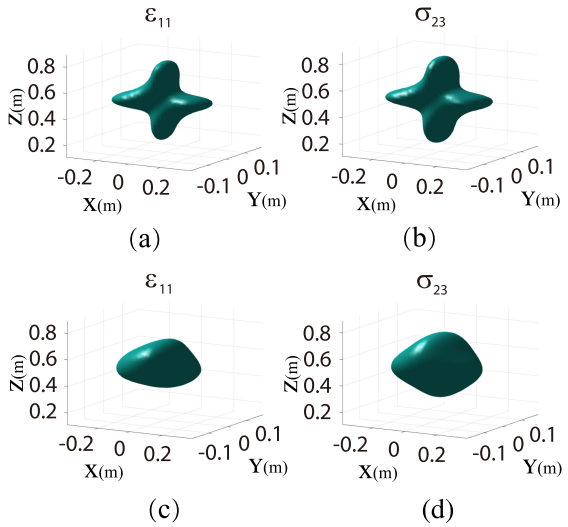

Fig. 4. 3-D isosurface plots of typical reconstructed dielectric parameters. (a) and (b) Plots based on the mixed L_1–L_2 norm regularization. (c) and (d) Plots based on the L_2 norm regularization. The isovalue is 1.6 for ε_{11} and 1.0 mS/m for σ_{23}.

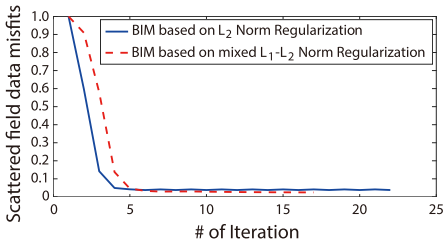

Fig. 5. Converging processes of BIM with the mixed L_1–L_2 norm and the L_2 norm regularization.

the inversion results is not taken into account. All the measured scattered field data are simulated by the BCGS-FFT solver. The regularization factor γ is empirically set as 4×10^{-3} and δ in $\mathbf{W}_i$ is set as 1×10^{-8}.

Figs. 2 and 3 show the 2-D slices of the reconstructed profiles of 12 anisotropic parameters based on the mixed L_1–L_2 norm regularization and the L_2 norm regularization, respectively. As can be seen, the geometric structures of each parameter are almost the same due to the mixed L_1–L_2 norm constraint. Moreover, due to the sparsity of the L_1 norm, the reconstructed background parameters are almost the same as the true parameters. However, since the mixed regularization can only make the parameters in a discretized cell be zero or nonzero simultaneously, it is impossible to guarantee the consistency of the geometric structure in the interior region of a scatterer. For example, the high-contrast region in the upper left of Fig. 2(b) is obviously different from that of the other parameters. As a comparison, the L_2 norm regularization obviously lacks the ability to constrain the shape of the scatterer among the different dielectric parameters, as shown in Fig. 3. In addition, the reconstructed scatterer volume is always larger than the true volume due to the loss of the shape constraint in the inversion based on the L_2 norm regularization. Consequently, the inverted dielectric parametric values are smaller than the true values. Fig. 4 shows the 3-D isosurfaces of typical reconstructed dielectric parameters based on mixed L_1–L_2 norm regularization and the L_2 norm regularization, respectively. The reconstructed 3-D shapes are almost the same for different parameters if we use the mixed L_1–L_2 norm. However, when the L_2 norm is adopted, not only the reconstructed shapes are different for different parameters, but they are also far from the true cross shape. In order to quantitatively evaluate the superiority of the mixed L_1–L_2 norm over the L_2 norm regularization, we use the structural similarity (SSIM) index, presented in [25], to quantify the similarity between the reconstructed profiles and the ground truth. The SSIMs based on two types of regularization are listed in Table II. The SSIMs between the parameters obtained based on the mixed L_1–L_2 norm and the ground truth exceed 0.8. This means they have at least 80% similarity. However, when the L_2 norm regularization is used, the similarity is between 50% and 63%. We also tried different values other than 4×10^{-3} for the regularization factor γ. It is shown that the regularization effect is not obvious if γ is too small. However, if γ is too large, the inversion error also becomes large. Meanwhile, the solution becomes too sparse due to the constraint by the L_1 norm. Similar numerical experiments have been performed to test the effects of different δ values. It is found that δ works normally as long as it is small enough. However, it leads to the distorted reconstructed shapes if it is too large, e.g., 0.1 in the numerical case. In addition, Fig. 5 compares the converging processes of the BIM with the mixed L_1–L_2 norm and the L_2 norm regularization. We can see that, although the SSIMs listed in Table II are quite different for two schemes, the convergence processes have no big difference since the same regularization factor is used.

IV. CONCLUSION

In this letter, the BIM with the mixed L_1–L_2 norm regularization is implemented to reconstruct the multiple dielectric parameters of anisotropic 3-D scatterers. The mixed L_1–L_2 norm is transformed into the L_2 norm via the weight matrix and the cost function of the BIM is easily minimized by the CG. Numerical results show that this regularization can make different dielectric parameters have similar geometrical structures in the inversion. Compared with the conventional L_2 norm regularization, the mixed L_1–L_2 norm can produce more accurate inversion results without additional computational cost. Finally, it is worth mentioning that the proposed mixed L_1–L_2 norm regularization can be applied to homogeneous background media, isotropic scatterers, scatterers placed across many background layers, or strong scattering scenarios although it is only validated by an anisotropic scatterer with the low contrast embedded inside a single layer.

REFERENCES

[1] P. M. Meaney, M. W. Fanning, D. Li, S. P. Poplack, and K. D. Paulsen, "A clinical prototype for active microwave imaging of the breast," *IEEE Trans. Microw. Theory Techn.*, vol. 48, no. 11, pp. 1841–1853, Nov. 2000.

[2] T. J. Cui, W. C. Chew, A. A. Aydiner, and S. Chen, "Inverse scattering of two-dimensional dielectric objects buried in a lossy Earth using the distorted born iterative method," *IEEE Trans. Geosci. Remote Sens.*, vol. 39, no. 2, pp. 339–346, Feb. 2001.

[3] L.-P. Song, C. Yu, and Q. H. Liu, "Through-wall imaging (TWI) by radar: 2-D tomographic results and analyses," *IEEE Trans. Geosci. Remote Sens.*, vol. 43, no. 12, pp. 2793–2798, Dec. 2005.

[4] Y. Zhong, M. Lambert, D. Lesselier, and X. Chen, "Electromagnetic response of anisotropic laminates to distributed sources," *IEEE Trans. Antennas Propag.*, vol. 62, no. 1, pp. 247–256, Jan. 2014.

[5] V. Sesetty and A. Ghassemi, "Effect of rock anisotropy on wellbore stresses and hydraulic fracture propagation," *Int. J. Rock Mech. Mining Sci.*, vol. 112, pp. 369–384, 2018.

[6] G. L. Wang, T. Barber, P. Wu, D. Allen, and A. Abubakar, "Fast inversion of triaxial induction data in dipping crossbedded formations," *Geophysics*, vol. 82, no. 2, pp. D 31–D45, 2017.

[7] F.-G. Hu, C.-F. Wang, and Y.-B. Gan, "Efficient calculation of electromagnetic scattering from cavities coated with bianisotropic media using FE–BI method with higher-order tetrahedral elements," in *Proc. IEEE Antennas Propag. Soc. Int. Symp.*, Albuquerque, NM, USA, Jul. 2006, pp. 3883–3886.

[8] R. A. Renaut, I. Hnetynková, and J. Mead, "Regularization parameter estimation for large-scale Tikhonov regularization using a priori information," *Comput. Statist. Data Anal.*, vol. 54, no. 12, pp. 3430–3445, 2010.

[9] Y. Chen, P. Wen, F. Han, N. Liu, H. Liu, and Q. H. Liu, "Three-dimensional reconstruction of objects embedded in spherically layered media using variational born iterative method," *IEEE Geosci. Remote Sens. Lett.*, vol. 14, no. 7, pp. 1037–1041, Jul. 2017.

[10] C. Estatico, M. Pastorino, and A. Randazzo, "A novel microwave imaging approach based on regularization in L^p Banach spaces," *IEEE Trans. Antennas Propag.*, vol. 60, no. 7, pp. 3373–3381, Jul. 2012.

[11] L. Pan, X. Chen, and S. P. Yeo, "A compressive-sensing-based phaseless imaging method for point-like dielectric objects," *IEEE Trans. Antennas Propag.*, vol. 60, no. 11, pp. 5472–5475, Nov. 2012.

[12] E. J. Candes and T. Tao, "Decoding by linear programming," *IEEE Trans. Inf. Theory*, vol. 51, no. 12, pp. 4203–4215, Dec. 2005.

[13] A. Abubaker and P. M. Van DenBerg, "Total variation as a multiplicative constraint for solving inverse problems," *IEEE Trans. Image Process.*, vol. 10, no. 9, pp. 1384–1392, Sep. 2001.

[14] P. Shah, U. K. Khankhoje, and M. Moghaddam, "Inverse scattering using a joint L_1-L_2 norm-based regularization," *IEEE Trans. Antennas Propag.*, vol. 64, no. 4, pp. 1373–1384, Apr. 2016.

[15] O. Portniaguine and M. S. Zhdanov, "Focusing geophysical inversion images," *Geophysics*, vol. 64, no. 3, pp. 874–887, 1999.

[16] O. Portniaguine and M. S. Zhdanov, "3-D magnetic inversion with data compression and image focusing," *Geophysics*, vol. 67, no. 5, pp. 1532–1541, 2002.

[17] L. E. Sun, "Parametric inversion of 3-D anisotropic permittivities from scattered electromagnetic fields," *IEEE Trans. Antennas Propag.*, vol. 66, no. 6, pp. 3027–3033, Jun. 2018.

[18] X. Millard and Q. H. Liu, "Simulation of near-surface detection of objects in layered media by the BCGS-FFT method," *IEEE Trans. Geosci. Remote Sens.*, vol. 42, no. 2, pp. 327–334, Feb. 2004.

[19] K. A. Michalski and J. R. Mosig, "Multilayered media Green's functions in integral equation formulations," *IEEE Trans. Antennas Propag.*, vol. 45, no. 3, pp. 508–519, Mar. 1997.

[20] J. Wang, J. Li, Y. Chen, F. Han, and Q. H. Liu, "Simulation of 3-D electromagnetic scattering and inverse scattering by arbitrary anisotropic dielectric objects embedded in layered arbitrary anisotropic media," *IEEE Trans. Antennas Propag.*, vol. 68, no. 8, pp. 6473–6478, Aug. 2020.

[21] J. Li, J. Zhuo, Z. Guan, F. Han, and Q. H. Liu, "3-D electromagnetic scattering and inverse scattering by magnetodielectric objects with arbitrary anisotropy in layered uniaxial media," *IEEE Trans. Antennas Propag.*, vol. 68, no. 2, pp. 1009–1022, Feb. 2020.

[22] F. Han, J. Zhuo, N. Liu, Y. Liu, H. Liu, and Q. H. Liu, "Fast solution of electromagnetic scattering for 3-D inhomogeneous anisotropic objects embedded in layered uniaxial media by the BCGS-FFT method," *IEEE Trans. Antennas Propag.*, vol. 67, no. 3, pp. 1748–1759, Mar. 2019.

[23] F. Li, Q. H. Liu, and L.-P. Song, "Three-dimensional reconstruction of objects buried in layered media using Born and distorted Born iterative methods," *IEEE Geosci. Remote Sens. Lett.*, vol. 1, no. 2, pp. 107–111, Apr. 2004.

[24] B. Wohlberg and P. Rodríguez, "An iteratively reweighted norm algorithm for minimization of total variation functionals," *IEEE Signal Process. Lett.*, vol. 14, no. 12, pp. 948–951, Dec. 2007.

[25] Z. Wang, A. C. Bovik, H. R. Sheikh, and E. P. Simoncelli, "Image quality assessment: From error visibility to structural similarity," *IEEE Trans. Image Process.*, vol. 13, no. 4, pp. 600–612, Apr. 2004.